The investigation of ancient metal artefacts by portable X-ray fluorescence devices

Journal:	*Journal of Analytical Atomic Spectrometry*
Manuscript ID:	JA-TRV-03-2014-000107.R1
Article Type:	Tutorial Review
Date Submitted by the Author:	03-Jul-2014
Complete List of Authors:	Ferretti, Marco; Institute for Technologies Applied to Cultural Heritage,

The investigation of ancient metal artefacts by portable X-ray fluorescence devices

Marco Ferretti

CNR – Istituto per le Tecnologie Applicate ai Beni Culturali

Via Salaria km 29.300, 00015 Montelibretti (Rome), Italy

Email: marco.ferretti@itabc.cnr.it

Abstract

X-ray fluorescence (XRF) analysis by portable spectrometers has long been applied to the study of ancient metal artefacts. Its effectiveness depends, on the one hand, on the capability of providing answers to archaeological, historical and technological questions. On the other, the artistic and monetary value of the artefacts is such that respecting the physical integrity of the objects is in most cases mandatory. These two conditions – *i.e.* being non-destructive and, at the same time, capable of significant results – affect the design of the spectrometer, with special regard to the balance between portability and analytical performance, as well as the measurement strategy. This paper presents a critical discussion concerning the use of portable XRF devices in the investigation of ancient metal artefacts, including the advantages and limitations of different technical solutions and measurement strategies.

Measuring the absolute composition of the objects often requires the removal of patina, which is seldom permitted for ancient artefacts. Hence, emphasis is given to alternative methods, more respectful of artefact integrity and capable to make the most of non-destructivity and measurement speed, which are the real mainstays of portable XRF. Other uses of this technique, such as the analysis of multilayered materials and the study of surface compositional changes are also discussed.

Introduction

This paper discusses different aspects of the application of portable X-ray fluorescence (XRF) to the investigation of ancient metal artefacts (Fig. 1). The focus is on the relationships between research questions, analysed materials, measurement strategies and instrumentation, which are considered as parts of a single 'knowledge-producing system'. Hardware components and quantification algorithms are considered as far as relevant to the user or the assembler of the equipment, but detailed technical specifications are beyond the scope of this paper.

For over fifty years, X-ray fluorescence (XRF) has been one of the most successful techniques used for the elemental analysis of cultural materials. The first case studies were published in the late 1950s[1] and the 1960s, when small metal objects[2-4], glass[5], jade[6] and pigments[7-11] were analysed by means of so-called wavelength-dispersive spectrometers, huge pieces of equipment that could not be moved from the laboratory. For the study of cultural materials the non-destructive nature of XRF was a much appreciated feature. However it could only be used on objects that were sufficiently small to fit in the measurement chamber and that could be brought to the laboratory. Bringing the XRF equipment to the object became possible in the early 1970's when the so-called energy-dispersive spectrometers, at that time equipped with detectors that had to be cooled by liquid nitrogen, came into widespread use. Thanks to the compact and open architecture of energy-dispersive systems, XRF spectrometers not only became portable and therefore suitable for *in situ* investigation[12,13], but it was also possible to extend their use to the analysis of objects of any shape and size.

Twenty years later, *in situ* usability of XRF spectrometers was further improved by the introduction of the so-called Si-PIN and Si-Drift detectors[14,15]. These detectors have

energy resolution similar to that attainable by liquid nitrogen cooling, but do not need liquid nitrogen. Together with low-power X-ray tubes, they made the construction of hand-held devices possible[16]. Such devices, built in a readily understood gun-like form are contributing much to the spread of portable systems and, at least in part, to the misperception that XRF is as easy as 'taking aim and shooting'. Since the early 70's, the size of the equipment has radically decreased, which means that the adjective 'portable' was originally used for equipment that today seems cumbersome. In this paper, 'portable' refers to any kind of spectrometer that can be used *in situ* and moved around the object.

The latest innovation in XRF equipment that has been significant for the analysis of cultural materials concerns poly-capillary optics[17,18]. These optics focus the excitation beam to some tens of μm and considerably improve the spatial resolution of the analysis, that is, the capability of analysing very small details with no interference from the surrounding materials. Should surface abrasion (discussed further below) be necessary for XRF analysis, a smaller abraded area is required, thus reducing the impact on the object.

The combination of non-destructivity and suitability for *in situ* use makes the XRF technique extremely effective in archaeometry and conservation science. It has provided significant results on a wide range of materials, even if the detection of the low atomic number component of these materials is difficult. Metal artefacts are ideal for applying XRF because all their major elements can be detected, with results that are often crucial in historical and technological research.

Physical principles and limitations of X-ray fluorescence

The physical principles of XRF are well known: if a sample is irradiated with electromagnetic radiation of suitable energy, electronic transitions can be induced in the inner shells of its atoms. Such transitions result in the emission of X-rays whose energy is characteristic of the element affected by the transitions, whereas the intensity of emission is related to its abundance in the sample.

As far as cultural materials are concerned, XRF has two important limitations. One is that the detection of low atomic number elements ($Z<20$) is difficult, due to their low photoelectric absorption coefficient, to the higher degree of internal conversion (Auger effect) and to the low energy of the characteristic radiation. The second limitation is that, due to the absorption of X-rays in the sample, only a relatively thin layer below the surface is analysed. A quantitative idea of where the analytical information comes from is given in Fig. 2. It plots the percentage of the overall fluorescent signal provided by the first *d* micrometres below the sample surface. The curves refer to an infinitely thick bronze alloy (85% Cu, 10% Sn, 5% Pb) and to the Cu-K, Sn-K and Pb-L fluorescent lines. Almost the entire analytical information of Cu and Pb and almost half of the Sn information comes from the first 20μm. If one considers that the corrosion products covering metal artefacts may easily reach several tens of μm in thickness, it is easy to understand how strongly corrosion limits the accuracy of XRF measurements.

A more general discussion of the interactions between the fluorescent radiation and the sample requires introducing matrix effect, which is the combination of absorption and enhancement (fluorescence excited in the analysed element by the fluorescent radiation of other elements in the sample). Given the scope of this paper, it is sufficient to say that matrix effect depends on the sample composition and that this dependence considerably complicates the relationship between the fluorescent intensity and the concentration of the analysed element.

Depending on the energy of the exciting radiation, different shells can be excited in the same element. Fig. 3 shows the spectrum of a bronze sample with 94.12% Cu, 2.3% Sn, 3.4% Pb, 0.03% Ag and 0.15% Sb, in which both the L- and the K-shells of Ag, Sn and Sb are excited. The energy span between the K-lines is much higher, which makes them more free from mutual interference and more suitable for quantification than the L-lines. In this spectrum, for example, the Sb Kα line can be easily distinguished from the adjacent Sn Kα, although the latter is 15 times more intense.

Elemental composition for understanding ancient metals

This section discusses how elemental analysis – and in particular portable XRF analysis – can contribute to the understanding of ancient metal artefacts, what metals can be investigated, with what results, to answer what questions.

For thousands of years – copper metallurgy began 8500 years ago in the Near East and 6500 years ago in Europe[19] – metals have played an important role in material cultures. Produced for the most diverse purposes, metal artefacts are extremely varied in shape, size and composition. Different combinations of casting, mechanical working and soldering produce objects with excellent mechanical properties, complex shapes and attractive appearance.

Whereas elemental composition is important in addressing archaeological, historical and technological issues, it must be considered that XRF is not equally effective for all metals. Characterization of iron alloys, for example, requires the analysis of low atomic number elements. They are present in such small amounts to be practically invisible to a portable XRF spectrometer[20]. In contrast, significant results have been obtained on copper, gold, silver and their alloys, as discussed below.

Copper-based artefacts are probably the most numerous class of ancient metal objects as they are relatively resistant to corrosion and common in everyday life. Depending on whether the main element alloyed with copper is tin or zinc, they are roughly classified as bronzes or brasses. Several minor elements occur in the composition of copper alloys, in sufficiently high amounts to be detectable by portable XRF. From the analyst's point of view, this is an advantage, not only because he/she has more variables to play with, but also because minor elements have larger variation ranges and are more effective discriminators than the major ones. A comprehensive overview on the composition of copper alloys, considering different types of objects, geographical contexts and historical periods, is provided by Craddock[21]. Though not decisive in determining the original context of an artefact – for example tin bronzes have similar compositions all over the Old World – elemental composition can be an indicator of the technical history of the object.

An example of the relationship between fabrication process and composition is given by composite artefacts in which some parts are cast and others are cold-worked, such as the handles and the basin in a vessel. The fabrication of a basin, as well as of any sheet of bronze, is done by hammering alternated with annealing, i.e. heating the piece to allow for relaxation of the stresses caused by hammering. Annealing is essential to restore the malleability of bronze, otherwise it would break before reaching its final shape. Fig. 4 plots analytical data from selected literature[21-28] concerning the Pb mass fraction in 280 artefacts, mostly vessels, from different cultural contexts (pre-Roman, Etruscan, Greek and Roman) and periods (7th century B.C. to 1st century A.D.). For each artefact, identified by a progressive number on the horizontal axis, black markers represent the cast parts and white markers the hammered ones. Most white markers are below the

corresponding black marker, meaning that, in the same object and independently on the absolute values, hammered parts always contain less Pb than the cast ones.

Whereas most authors assume that such a difference is intentional, Ferretti *et al.*[29] observed that the cycles of hammering and annealing may produce a spontaneous and qualitatively similar effect. Fig. 5 is a scanning electron microscope (SEM) back-scattered electron (BSE) image of a cross-section and shows the effect of annealing on a leaded bronze. At temperatures of 600-700°C, Pb is liquid in a solid Cu-Sn matrix and tends to migrate towards the surface. There, it is absorbed by the spongy cupric oxide (CuO, tenorite) formed at high temperature and oxidized. This process, repeated many times during the fabrication, may cause – at least in part – the low Pb content observed in hammered pieces. Observations of Van Langh *et al.*[30], describing the effect of heating on the XRF analysis of Pb in Cu alloys, can be related to this phenomenon.

Copper-based alloys are frequently covered by layers of corrosion products, commonly called patina (a corrosion layer which retains the form of the original surface of the object), reaching several tens or hundreds of μm in thickness. Robbiola *et al.*[31] show that, in burial contexts where water is present, corrosion takes place by selective dissolution of Cu from the alloy. Copper corrosion products tend to leave the surface of the object, as they are more soluble than those of Sn and Pb. According to whether the original surface is preserved or not, Robbiola *et al.* identify a type I corrosion, characterised by low corrosion rates and a Sn content similar to that of the bulk alloy, and a type II corrosion, characterised by a generalized corrosive attack and Sn content higher than in the bulk alloy.

Residual stress may affect corrosion as well. For example, Ferretti *et al.*[32] observed that cold-worked pieces have their own corrosion pattern. This is characterised by a compact, protective layer of tin oxide (SnO_2, cassiterite) produced by the anodic

behaviour of the areas affected by residual stress. Similarly to type II corrosion, the Sn content is higher than that of the bulk alloy but, in contrast to it, the corrosion layer retains the morphology of the original surface.

High fluorescent intensities (or apparent concentrations) of Sn can be used as indicators of deep corrosion. This will be further discussed in the next section.

Gold alloys can disclose important information through elemental analysis[33]. For example, Pt and Pd can be used to distinguish gold ores and detect changes in gold supplies; native gold can be recognised from composition; the Ag-Pb correlation indicates intentional alloying of gold and silver; different soldering techniques can be distinguished through Cu and Ag contents.

Elemental analysis of silver alloys is less informative, as purification processes may remove ore-characteristic trace elements from the metal.

Both gold and silver are used in the manufacturing of "coated" artefacts and, once again, elemental analysis is important to address technological questions. The presence of Hg, for example, is characteristic of the fire gilding technique, whereas variable Hg/Au ratios on the same object may indicate different phases in the application of the amalgam or even different craftsmen.

Corrosion does not occur in gold artefacts, which makes them ideal, as to measurement accuracy, for XRF applications. This is not the case of Ag alloys, in which the presence of corrosion products, mainly acanthite (Ag_2S) and chlorargyrite (AgCl), interferes with the measurements and causes problems similar to those of Cu alloys.

Measurement strategies for using portable XRF devices

Analytical approaches aimed at quantification of chemical elements were the first and, probably, the most practised applications of XRF analysis in study of ancient metal

artefacts. They consist in measuring the absolute composition of the alloy with the best possible accuracy and precision. As accuracy is worsened by the presence of corrosion products on the object surface, these have to be removed prior to XRF analysis to expose the uncorroded metal (which is not always feasible given the cultural and monetary value of the artefacts). An example of quantification performed by portable XRF on gold, silver and copper alloys is provided by Karydas[34].

One of the main advantages of quantification-aimed approaches is that they allow for comparing and pooling data generated by different laboratories, provided the measurements are reproducible. The results of an inter-laboratory comparison carried out by Heginbotham *et al.*[35] show that, in fact, they are not or, at least, not yet reproducible. The comparison established that reproducibility of portable XRF measurements on copper alloys is higher than 50% relative for all elements, except Cu, Zn, and Sn. This is hardly satisfactory, at least from the point of view of a quantification-oriented analyst, but is inherent in portable equipment. Moreover the comparison was carried out on polished samples, whereas real life objects are corroded, which further increases the overall uncertainty. One has to wonder if accurate and precise analyses on ancient metal objects are a realistic goal.

Aside from that, a crucial question is if quantification is really needed. Will knowing the 'true' concentration of a given element actually affect the archaeological, historical and technological conclusions? It has been shown that this occurs with gold alloys, but the concentration ranges of the most significant elements are below the detection limits of portable XRF, so that this technique is not (yet) applicable[33].

The case of copper alloys is even more complicated: given the compositional spread reported by Craddock[21], it seems unlikely that quantification can be decisive in solving historical problems. It is true that composition is related to the technical history of the

object, but such relationship is in most cases qualitative. For example, Fig. 4 shows that, in the same object, hammered parts contain less lead than cast parts, but there is no threshold below which a piece can only be hammered and above which it can only be cast. Moreover, copper alloys are not so prone to quantification, as the accuracy is strongly affected by surface corrosion. For many years[36], the removal of patina is a common means of reaching the uncorroded metal, thus avoiding the problem. This practice, however, is not advisable because: a) patina may retain morphological details of the original surface; b) it may be protective and prevent further corrosion and c) it may be difficult to know when to stop abrading, as a shiny aspect does not guarantee that uncorroded metal has been reached. Besides being of uncertain success, the removal of patina is always an irreversible alteration of the integrity of an object.

It can be concluded that measuring the absolute composition of a metal artefact is not the most profitable use of portable XRF. The real mainstay of this technique is a combination of non-destructivity and measurement speed. A different, alternative approach making the most of these capabilities is possible and will be discussed below. Such an approach assumes that the measurement is carried out on the unaltered surface, that is to say, no patina is removed by the analyst. The discussion that follows is for copper alloys, because they provide the most adverse measurement conditions. The principle, however, can be applied to other types of alloys as well.

One of the advantages of a non-destructive method is that the number of measurements can be high – virtually infinite – with no consequences for the object and short measuring times make multiple measurements feasible. In the highly variable conditions typical of ancient metal artefacts, working with clusters, instead of single data points, has the obvious advantage of allowing identification of average behaviours and outliers. It is worth remarking that this is opposite to a quantification-aimed approach, in which

the damage caused by surface abrasion necessarily restricts the number of measurements.

Fig. 6 shows a simulation obtained by the fundamental parameters (see next section) software PyMCA[37]. It represents the fluorescent behaviour of a bronze substrate (88% Cu, 10% Sn, 2% Pb) covered by two different types of corrosion layers of variable thickness, corresponding to Robbiola's type I and type II corrosion[31]. The relative variations in the fluorescent intensities are plotted versus the thickness of these layers. In more detail, the relative intensity is defined as $RI(t)=I_{i,j}(t)/I_{i,0}$, where t is the coating thickness, $I_{i,j}(t)$ is the fluorescent intensity from the substrate and the corrosion layer, and $I_{i,0}$ is the fluorescent intensity from the substrate alone, the index i accounting for Cu-Kα, Sn-Kα or Pb-Lα, and the index j accounting for type I or type II corrosion. These are simulated through a homogeneous mixture of corrosion products, whose composition is calculated according to reference 31 and given in Tab. 1. The model shows two aspects that are observed in real cases. One is that the corrosion layer causes an inverse relationship between the fluorescent intensity of Cu and those of Sn and Pb. The second relevant aspect is that the concentration of Sn (and Pb) observed on the corroded surface may be several times higher than in the bulk. It increases as the corrosion layer gets thicker and the corrosion pattern moves towards the more destructive type II.

As the presence of corrosion interferes with the measurement, it is essential to choose measurement areas with the thinnest possible patina. Besides visual recognition, which is a skill that the analyst learns by working together with other professionals such as conservator-restorers, an important indicator is the apparent concentrations of Sn: the lower, the better. Thus XRF can inform condition assessment.

Measurements on the corroded surface are made on the assumption that it retains at least part of the compositional information from the bulk metal. To understand if and to what extent this is true, it is useful to look at the results obtained by repeating the measurement in different areas of the same piece. Fig. 7 plots the Sn versus Sb K-lines intensities measured on an actual artefact made of five separate pieces, identified as alloys A, B, C, D and E. For each of them, the intensities vary by a factor of 2-3 and are therefore unusable for quantification. Within the same piece, however, the data points show a clear correlation. If one assumes that the variations in the fluorescent intensities are mainly due to the variations in the thickness of the corrosion layer, then the two elements must have undergone similar enrichment or depletion effects in the corrosion process. One can therefore conclude that the Sb/Sn ratio, as measured on the corroded surface, is not too far from that of the uncorroded metal. Here, it can be used to distinguish three different compositional groups: one is made by alloys A, B and C, one by alloy D and one by alloy E.

One can check how general these conclusions are on a database of about 2500 XRF measurements concerning objects from Greek and Italian geographical contexts, dating from the 11th century B.C to the 17th century A.D. Inter-element correlations are calculated within the group of measurements performed on each of the approximately 100 different alloys, identified in the database.

It is important to note that the measurements are biased. One reason is that all the artefacts were analysed after restoration, that is, loose corrosion products had been removed and only the stable ones had been left. The second reason is that selection of the measurement points is not random: as mentioned above, areas with the thinnest possible corrosion layer were selected, compatible with the need of representing all the constituent alloys of the artefact.

Fig. 8 shows the histograms of the inter-element correlation coefficients. The K-lines are considered for Cu, As, Ag, Sn, Sb and the L-lines for Pb. The fact that the analytical volume changes with the energy of the fluorescent radiation contributes to worsen the correlation. Not surprisingly, the Sn-Sb histogram is the clearest one: the fluorescent energies of these elements are similar, which involves the same attenuation and the same analytical volume. The histogram shows that the Sn-Sb correlation is in most cases positive and high, that is, the conclusions of the case study in Fig. 7 can be generalised. A similar, though less sharp, behaviour is shown by Ag and, to some extent, by As, although the latter suffers from the spectral interference – and positive correlation – with Pb. The frequent negative Cu-Sn and Cu-Pb correlations are consistent with Robbiola *et al.*[31]: the concentration of Sn and Pb increase as Cu is dissolved and removed from the surface.

The general conclusion is that at least three elements, *i.e.* Sn, Sb and Ag, have similar behaviours in the corrosion process, that is, the mutual ratios in the corrosion layer remain reasonably similar to those of the uncorroded metal and can be used to fingerprint the alloy. As Sb and Ag are usually present in minor amounts, good detection limits for medium atomic number elements are required.

It is clear that the approach so far discussed, often called ‘pattern-recognition’, is suitable to highlight differences, but not to measure absolute compositions. This application of XRF analysis was first used to confirm the hypothesis that three legs of the Capitoline Horse had been replaced in ancient times[38]. As it was the first case study, there was no means of comparing the Sn-Sb correlation with that of other case studies. Nevertheless, if one considered the distances between the clusters and the homogeneous patina having a reasonably systematic effect all over the dataset, it was clear that the differences observed in the fluorescent intensities could not be simply ascribed to the

effect of corrosion. Fig. 9 represents the results: the fluorescent intensities of Sn and Sb alone are sufficient to show that some parts of the sculpture, namely three of the legs, the brow and the tail, are not of the same alloy as the body and, possibly, not original. The correlation between Sn and Sb is clear, as well as the fact that minor elements have more discriminating power than the major ones, mainly due to higher variation ranges. Here the Sb fluorescent intensity varies by a factor of 20 between the original and the non-original parts. The outliers, here marked with a grey circle, can be easily identified. These results are consistent with Craddock's analyses (ref. 21, tab. 33 of the attached microfiches), noted in Tab. 2. The difference between the analytical approaches is outstanding: Craddock was focused on the alloys' composition, but – possibly due to restrictions in sampling – he had not a complete compositional picture of the object and only recognised one among several non-original parts (*i.e.* the hoof as part of the front right leg). Conversely, Ferretti *et al.* could not provide the composition of the alloys, but 'sniffed' the whole surface of the sculpture and identified all the parts differing in composition from the original alloy. This case study also shows that XRF analytical information can be quantitative without necessarily aiming at element quantification.This approach has also been used to ascribe loose parts or fragments to a given artefact[39-41], to study the recycling of parts from pre-existing objects[42,43], to highlight casting sequences in the fabrication of complex artefacts[41,44,45], and to study the use of different alloys to obtain chromatic effects[46].

Other applications of portable XRF concern the analysis of bi-layered structures (a substrate and a coating), which are relatively common in ancient metal artefacts. Though not comparable with the examination of a cross-section as to the amount of information achieved, XRF methods are non-destructive and may be the only viable option for valuable artefacts in some cases. The principle is based on the relationship

existing between the coating thickness and the fluorescent intensity of a suitable element in the substrate. Cesareo *et al.*[47] discuss the theoretical background and the application to Giotto's halos in the Scrovegni Chapel in Padua (Italy) and to gilded copper objects from both the Royal Tombs of Sipán and the Museum of Sicán in Peru. Starting from the same background, Ferretti *et al.*[48] propose a method based on fundamental parameters' calculations solely, with no need for thickness calibration. It is *ad hoc* developed for gilded and enamelled silver artefacts and relies on the relationship existing between the coating thickness and the ratio Kα/Kβ of the substrate silver. The excitation efficiency of Ag is maximised by the X-ray tube working at 60kV.

The method has been applied to the four processional crosses of Borbona, Sant'Elpidio, Rosciolo and Forcella – Abruzzi area (Italy), first half of the XIVth century A.D. – made of gilded and embossed silver sheets and decorated with enamelled silver plates. Fire gilding was immediately recognised due to the presence of Hg, as well as ancient restorations due to the higher Cu content. More unexpected was the variability in the Au/Hg ratio observed in one of the crosses. It led to the supposition that different parts of the artefact were gilded by different executors, which is consistent with the historical hypothesis that, within the workshop, the master made the main characters, whereas the pupils attended to less important parts. The enamels were investigated by the same method, except that, due to the difficulty in detecting low atomic number elements, only colourants and opacifiers could be analysed. Particularly significant is the composition of the blue enamels, characterised by Co with minor amounts of Zn, Pb and In. The presence of such impurities is typical of blue glasses from the 12th to 14th century A.D. and is related to the source of Co minerals.

The sensitivity of XRF to near-surface composition, which is usually considered a drawback, proves useful to monitor the changes caused, for example, by thermal

treatments. Ferretti *et al.*[49] investigated the mechanisms of surface silver enrichment observed in *nummi*, a type of late Roman coin made of bronze with 2-6% Sn, 1-6% Pb and 1-4% Ag. Part of the fabrication sequence was reproduced on *ad hoc* prepared specimens simulating (in composition) the alloys of the original *nummi*. The idea was to verify the hypothesis – already formulated by Cope[50] – that heating the blank (to facilitate striking) causes Pb to melt and carry the Ag contained in the alloy towards the surface. The mechanism is similar to that of Pb migration described in a previous part of this paper. The specimens contained the same amount of Sn (5%) and Ag (3%) but different amounts of Pb (1-10%) to highlight the role of this element in the process. They were heated at 700°C, then cooled and pickled in acetic acid.

Fig. 10 shows (from top to bottom) the SEM-BSE image, the Ag map and the Pb map of a specimen after heating, no pickling having been done yet. It is observed that, at reaching the surface, Pb takes the outer position, while Ag keeps closer to the bulk metal.

Whereas the image qualitatively confirms the hypothesis, it is difficult to extract any global quantitative information. It was therefore decided to use portable XRF to obtain average figures significant of the whole specimen. Fig. 11 shows the scatterplots of the areas of Pb Lα (top) and Ag L (bottom) lines versus the different Pb content of the alloys, for untreated, heated and pickled specimens, respectively. It is observed that surface Pb content increases after heating and decreases after pickling (which proves that Pb is in the oxidised state and is effectively removed by acetic acid). Conversely Ag fluorescent radiation, which is shielded by the overlaying Pb, increases in intensity when the latter is removed. It is also observed that Ag fluorescent intensity is an increasing function of the Pb content in the alloy, that is, the higher the Pb content, the more efficient the transport of Ag. Once again, this example shows that there are

quantitative ways of using XRF analytical information other than measuring the absolute composition.

Instrumentation and quantification algorithms

This section discusses the hardware components with a focus on the key features that need to be considered when purchasing (or assembling) a portable XRF device. Besides weight and size, which are key features of portability, these are measuring time and detection limits. A general discussion of quantification algorithms is presented, although the author does not consider quantitative analysis the best use one can make of portable XRF.

A typical energy-dispersive XRF experimental setup is shown in Fig. 12: the main components are the excitation source, the detector, the systems for pulse processing and spectrum acquisition and the computing system for spectrum processing and quantification.

The source provides the exciting, or primary, radiation. Good detection limits and short measuring times require the highest possible radiation output, compatible with the need to avoid detector saturation. Though in principle both radioactive sources and X-ray tubes can be used, the higher radiation output leads, in most cases, to opt for the latter. X-ray fluorescence is a threshold phenomenon, that is, a given element can be analysed only if the energy of the exciting radiation is higher than that of the absorption edge of the element itself. The energy distribution of the primary radiation becomes therefore crucial. Depending on the anode material (Cu, Mo, Pd, Rh, Ag, Ta, W, Au anodes are commonly used) and on the voltage at which the tube is operated, it may either be peaked on the anode fluorescent energies or have a broad (bremsstrahlung) spectrum. The former option provides a lower background, but is unsuitable to excite the K-shells

of medium atomic number elements (see Fig. 3). Conversely, the latter can be excited with good efficiency if the X-ray tube has a W anode and is operated at 50-60kV. In such conditions the primary radiation has a broad spectrum with a relatively intense component above 30-35keV. Sheets of metal can be placed on the beam path to absorb the low energy component and optimise the background in the region of interest.

The detector is the device in which the energy of the fluorescent radiation is absorbed and converted into electrical pulses. The absorbing medium is a semiconductor in all detectors used for portable XRF. Three main types are discussed here: a) silicon and germanium detectors requiring liquid nitrogen cooling, b) silicon diodes (Si-PIN) and c) silicon drift (Si-Drift) detectors. Type a) and b) detectors are smaller in size and do not require liquid nitrogen cooling. They are now used in all portable systems. In order to compare their performance, it is useful to consider three key parameters, that is, efficiency, energy resolution and count-rate capability.

Efficiency accounts for how much of the fluoresced radiation is actually detected and consists of two components. One, called geometric efficiency, is related to the solid angle subtended by the detector and increases with the area. It is almost irrelevant for the overall performance because a large detector has to stay further away, whereas a small detector can get closer to the sample. In the end, the subtended solid angle is more or less the same. The second, and far more important, component is the so-called energy (or intrinsic) efficiency. It accounts for the capability to stop the fluorescent radiation within the active volume of the detector and depends on its material and thickness. For example, nitrogen-cooled Si(Li) detectors have a thickness of several mm. This provides an energy efficiency not far from 100% at the energies of practical interest in the analysis of ancient metal artefacts (25-30keV). Conversely, the thickness of Si-PIN

and Si-Drift detectors is about 500μm and the energy efficiency at 25-30keV is about 20%.

Noise is a major problem in radiation detectors because it affects energy resolution, that is, the capability of distinguishing between lines of similar energy. It depends on a complex combination of parameters. One is the active volume: the higher the volume, the higher the noise from thermal excitation. This explains why large-sized detectors need to be cooled by liquid nitrogen at -200°C, whereas small Si-PIN and Si-Drift detectors obtain approximately the same resolution at -20°C by thermo-electrical cooling.

A parameter that can be optimised to some extent to reduce noise is the time constant of the amplifier, or shaping time. At high shaping times, the amplifier acts as a low-pass filter and cuts the high-frequency noise, thus improving the energy resolution. Unfortunately, it also increases the pulse duration and the pile-up of successive pulses, thus worsening the count-rate capability. For each type of detector, one has therefore to find a balance between the opposite requirements of reducing noise and increasing speed.

Energy resolution is by convention measured as the full width at half maximum (FWHM) of the Mn Kα-line (5.9keV). Although it is often used by the manufacturers as 'the' figure of merit for the detector performance, the user should be aware that energy resolution cannot be considered separately from count-rate capability, as no improvement of the former can be obtained without detriment to the latter. Moreover, there is no need for extreme performances, as 160-180eV are more than enough for the analysis of ancient metal artefacts and for many other applications. Tab. 3 shows typical figures for nitrogen-cooled Si(Li), Si-PIN and Si-Drift detectors[51-56]. It can be observed that Si-Drift detectors achieve the same energy resolution as nitrogen-cooled Si(Li) and

Si-PIN detectors with considerably shorter shaping times. This is due to a unique electrode structure that provides lower noise, more effective charge collection and ensures a count-rate capability 10 to 100 times higher.

This feature makes Si-Drift detector most suited to work with high intensity sources. Among the other advantages, high count-rates balance the low energy efficiency at 25-30keV and provide good statistics also for the K-lines of medium atomic number elements.

Several spectral artefacts are observed in Si-PIN and Si-Drift detectors. To reduce interactions at the edges of the active volume, both are equipped with built-in collimators, whose fluorescent radiation interferes with the sample spectrum[57]. At the higher count-rates achievable with a Si-Drift detector, further artefacts are due to the sum peaks, that is, two photons are detected at the same time and seen as a single photon with energy equal to the sum of the energies. Fig. 13 shows the spectrum of pure Cu, taken with a 30mm^2 Si-Drift detector with Mo collimator and digital pulse processing. Besides the sample fluorescent lines (*i.e.* the K-lines of Cu), the spectrum is contaminated by the K-lines of the Mo collimator and by the sum peaks of Cu.

Combining the right source with the right detector is crucial for the performance of a portable XRF device. When portability is a priority, small-sized, low power (and low photon output) tubes are the best option. Here the count-rate capability is irrelevant, which allows the use of Si-PIN detectors. Conversely, if the priority is analytical performance, a tube with high photon output is required, with consequently increased needs for cooling and shielding. Also, the count-rate capability of the detector has to be consistent with the high excitation rate, which leads to Si-Drift detectors as the only possible choice.

In order to compare the analytical performance of a different combination of components, a survey on detection limits – assumed indicative of the performance itself – was carried out among portable XRF users in Spain and Italy[58]. A 50 eurocents coin (Cu 89%, Al 5%, Zn 5%, Sn 1%) was used as reference material, in order to reveal the analytical performance for elements in both Z≈30 and Z≈50 ranges. Fig. 14 compares, on a logarithmic scale, the detection limits of the participant systems. The X-ray tube working parameters and the type of detector are synthetically reported on the horizontal axis. The ranges are 50-300μg/g for Zn and 20-1500μg/g for Sn, for a measuring time of 300s. As expected, using X-ray tubes working at 50-60kV is beneficial for detection limits, in particular for Sn. However, they increase the weight of the equipment, reducing its portability.

When purchasing a portable XRF device and considering different options, it is advisable to use a reference material (for example the coin mentioned above) to compare the count-rates of Sn: the higher the better, at least as far as analytical performance is concerned. This is a means of assessing suitable excitation of the K-lines of medium atomic number elements, so important in the investigation of ancient metal artefacts.

Pulse processing is performed by an amplifier (also called shaper) and consists in shaping and optimizing for counting the electric pulses generated in the detector. Most of what the user has to know about pulse processing has already been discussed when dealing with energy resolution. Afterwards, a multichannel analyser classifies the pulses according to their amplitude and builds the spectrum. Pulse processing can be either analogue or digital. In the former case, the shaping time and the energy range of the spectrum are fixed by the manufacturer. Conversely, digital pulse processing offers the

possibility to adjust both parameters and enables the user to establish his/her own balance between energy resolution and count-rate capability.

The last important piece of hardware that has to be considered is the stand, i.e. the device used to keep the spectrometer in the measuring position. It is not part of the spectrometer, but it determines what parts of the artefact can be reached and analysed (see Fig. 1). A mechanically stable and easily adjustable stand can be bulky and pose more problems of portability than the spectrometer itself.

Spectrum processing and quantification – *i.e.* deriving the analyte concentration from the fluorescent intensity – are performed by a computing system. Different methods are used for quantification[59]. Depending on the way of dealing with matrix effect, they can be broadly divided into two types: a) empirical methods – also called influence coefficients methods – based on experimental curves obtained with calibration standards; and, b) theoretical methods – also called fundamental parameters (FP) methods – based on mathematical models. Combinations of the two approaches are also possible.

Empirical methods are potentially capable of the highest accuracies. They are grounded on the assumption that the standards are in every way similar to the unknowns, which on one hand limits their validity to the concentration ranges covered by the standards and, on the other, is clearly difficult to achieve with such unpredictable materials as ancient metal artefacts. A further drawback is that empirical methods cannot deal with multilayered structures.

Theoretical methods perform quantification by comparing the experimental spectrum with a theoretical one, obtained from the mathematical description of the sample-spectrometer system. As they rely on mathematical models, these methods retain their validity over a wide range of concentrations and are therefore more flexible. Accuracy

depends on the uncertainty with which the parameters that describe the sample-spectrometer system are known. An important feature of theoretical methods, at least as far as ancient metal artefacts are concerned, is that they can deal with multilayered materials.

In principle, these methods can be calibrated by means of a single standard, which allows accounting for the intensity of the primary radiation and the geometry factors. All the other parameters are supposedly known. In real cases, however, the inevitable inaccuracies in describing the primary spectrum and the energy efficiency of the detector make the use of several standards advisable.

Both FP and empirical methods depend on calibration standards to correct for the physical effects caused by the surface conditions of the sample. In fact, the difficulty in making the standards similar to the unknowns leads to a paradoxical reverse approach, that is, making ancient metal objects similar to the standards by abrading their surface.

A variant of the FP methods, virtually able to overcome the difficulties presented by inhomogeneous and irregularly shaped materials, are the Monte Carlo methods[59,60]. They seem therefore promising to solve some important problems related to the analysis of ancient metal artefacts. Based on a statistical description of the interactions rather than on deterministic equations, they are potentially able to account for all the physical phenomena, provided the corresponding probability density functions are known. Accuracy, however, depends on the number of histories considered. With the present computer technology, they require long computing times and are therefore unsuitable to process large datasets.

Conclusions

This paper has considered different aspects related to the use of portable XRF devices for the investigation of ancient metal artefacts; these are summarised in Fig. 15. It has been shown that these aspects are connected with the context that provides the objects and the research questions (i.e. the world of conservation, archaeology and the history of art), and with the conditions in which the investigation takes place. As a source of questions, archaeology is inevitably connected with the conservation of artefacts, which puts further conditions – for example respecting the physical integrity of the objects – but also contributes with the conservators' knowledge, deriving from extended visual and physical contact with the artefact.

The measurement strategy has to be consistent with the nature and the context of the investigated materials. Accurate quantification often requires abrading part of the surface to access the bulk metal and therefore conflicts with the conservation ethos of non-destructivity, which is mandatory in most cases. Hence, the need for approaches, alternative to the quantification-oriented ones, that do not require abrasion.

In every day life, most analytical questions require establishing differences, rather than measuring absolute compositions. To do so, this paper has discussed approaches in which compositional comparisons are performed by considering the relative position of clusters of data points in the space of the count-rates. It has been shown that this is possible for copper-based artefacts because Sn, Sb and Ag have similar corrosion histories. Therefore, the mutual ratios that they have in the corrosion layer are reasonably similar to those of the uncorroded metal and can be used to distinguish alloys from one another. The method has proved effective to identify non-original parts, to ascribe loose parts or fragments, to study recycling practices, and to follow casting sequences.

Portable XRF spectrometers are also used to analyse multilayered materials and derive both the composition and the thickness of the layers. The attenuation of the Ag K-lines from the substrate, for example, can be used to measure the gilding or the enamel thickness in gilded and enamelled silver artefacts. Finally it has been shown that the sensitivity of XRF to near-surface inhomogeneities proves effective to study surface compositional changes due, for example, to thermal treatments.

The design of a portable XRF spectrometer also has to be compatible with the nature and the context of the investigated materials. Portability is only one of the features that influence the effectiveness and usability of an instrument. Analytical performance is equally important. As they conflict with each other, the designer has to achieve a balance that is largely arbitrary. The author's preference is clearly in favour of analytical performance: the method for compositional comparison proposed in this paper is possible only thanks to good detection limits.

Acknowlegements

I am grateful to Giuseppe Guida (ISCR, Roma), Susanne Plattner (Dept. of Chemistry, University "Sapienza", Roma), Francesco Paolo Romano (CNR-IBAM, Catania) for the technical discussions on corrosion and radiation detectors, and to Claudia Polese (INFN-LNF, Frascati) for the calculations in XRF models.

I am also grateful to Dinah Eastop (Conservation Consultant, London), José Luiz Pedersoli Júnior (Scientia pro Cultura, Belo Horizonte), and Katriina Similä (ICCROM, Roma) for reading and commenting the paper and for revising the English.

References

1 E.T. Hall, *Year Book of the Physical Society*, 1958, 22-34.

2 C.M. Kraay, *Archaeometry*, 1958, **1**, 21-23.

3 C.H.V. Sutherland and M.R. Harold, *Archaeometry,* 1961, **4**, 56-61.

4 E.T. Hall and G. Roberts, *Archaeometry*, 1962, **5**, 28-32.

5 M. Banks, N. Elphinstone and E.T. Hall, *Archaeometry*, 1963, **6**, 26-30.

6 E.T. Hall, M.S. Banks and J.M. Stern, *Archaeometry*, 1964, **7**, 84-89.

7 R.J. Gettens and E. West Fitzhugh, *Stud Conserv*, 1966, **11**, 54-61.

8 J. Plesters, *Stud Conserv*, 1966, **11**, 62.

9 R.J. Gettens, H. Kuhn and W.T. Chase, *Stud Conserv*, 1967, **12**, 125-139.

10 H. Kühn, *Stud Conserv*, 1968, **13**, 7-33.

11 B. Mühlethaler and J. Thissen, *Stud Conserv*, 1969, **14**, 47-61.

12 R. Cesareo, F.V. Frazzoli, C. Mancini, S. Sciuti, M. Marabelli, P. Mora, P. Rotondi and G. Urbani, *Archaeometry*, 1972, **14**, 65-78.

13 E.T. Hall, F. Schweizer and P.A. Toller, *Archaeometry*, 1973, **15**, 53-78.

14 A.C. Huber, J.A. Pantazis and V.T. Jordanov, *Nucl Instrum Meth B*, 1995, **99**, 665-668.

15 P. Lechner, S. Eckbauer, R. Hartmann, S. Krisch, D. Hauff, R. Richter, H. Soltau, L. Strüder, C. Fiorini, E. Gatti, A. Longoni and M. Sampietro, *Nucl Instrum Meth A*, 1996, **377**, 346-351.

16 S. Tohyama and S. Piorek, in *Encyclopedia of Analytical Chemistry*, John Wiley & Sons, 2014, pp. 1-24.

17 M.A. Kumakhov, *X-Ray Spectrom*, 2000, **29**, 343-348.

18 A. Rindby and K.H.A. Janssens, in *Handbook of X-Ray Spectrometry*, ed. R.E. Van Grieken and A.A. Markowicz, Marcel Dekker, New York, 2nd edn., 2002, 643-729.

19 R.F. Tylecote *The early history of metallurgy in Europe,* Longman, London, 1987, 3-11.

20 Ch. Degrigny, A.G. Karydas, S. Golfomistsou, V. Kantarelou, C. Zarkadas and D. Vella, Proceedings of Metal 07, Amsterdam, 2007.

21 P.T. Craddock, Proceedings of Application of Science in Examination of Works of Art, Boston, 1985, attached microfiches.

22 J. Riederer, in Proceedings of 6th Tagung uber antike Bronzen, Berlin, 1980.

23 J. Riederer, in *Die Alamannenbeute aus dem Rhein bei Neupotz*, ed. E. Künzl, Mainz, 1993, pp. 407-46.

24 J. Riederer, in *The Bronze vessel 2. Description of the Provincial Museum G. M. Kam at Nijmegen*, ed. A. Koster, 1997, vol. XIII, pp. 95-106.

25 J. Riederer, *Rathgen-Laborbericth*, 1998, **19**.

26 J. Riederer, in *I grandi bronzi antichi: le fonderie e le tecniche di lavorazione dall'età arcaica al Rinascimento: atti dei seminari di studi ed esperimenti*, ed. E. Formigli, Nuova immagine, Siena, 1999, pp. 271-274.

27 J. Riederer in *Proceedings of XV Congresso Internazionale sui Bronzi Antichi*, Monique Mergoil, Montagnac, 2002, vol. 21, 284-91.

28 C. Iaia, *Produzioni toreutiche della prima età del ferro in Italia Centro-Settentrionale. Stili decorativi, circolazione, significato*, Istituti Editoriali e Poligrafici Internazionali, Pisa-Roma, 2005, vol. 40.

29 M. Ferretti, G. Guida, A. Manda and F. Milazzo, unpublished work.

30 R. van Langh, A. Pappot, S. Creange, L. Megens and I. Joosten, Proceedings of Metal 2010, Charleston, 2010.

31 L. Robbiola, J.-M. Blengino and C. Fiaud, *Corros Sci*, 1998, **40**, 2083-2111.

32 M. Ferretti, G. Guida and F. Volpi, unpublished work.

33 M.F. Guerra, in *Radiation in Art and Archaeometry*, ed. D.C. Creagh and D.A. Bradley, Elsevier, Amsterdam, 2000, pp. 378-416.

34 A.G. Karydas, *Ann Chim-Rome*, 2007, **97**, 419-432.

35 A. Heginbotham, A. Bezur, M. Bouchard, J.M. Davis, K. Eremin, J.H. Frantz, L. Glinsman, L-A. Hayek, D. Hook, V. Kantarelou, A.G. Karydas, L. Lee, J. Mass, C. Matsen, B. McCarthy, M. McGath, A. Shugar, J. Sirois, D. Smith and R.J. Speakman, Proceedings of Metal 2010, Charleston, 2010.

36 G.F. Carter, *Archaeometry*, 1964, **7**, 106-113.

37 V.A. Solé, E. Papillon, M. Cotte, Ph. Walter and J. Susini, *Spectrochim Acta B*, 2007, **62**, 63-68.

38 M. Ferretti, L. Miazzo and P. Moioli, *Stud Conserv*, 1997, **42**, 241-246.

39 M. Ferretti, E. Formigli, L. Lepore, F. Lo Schiavo, E. Macnamara, M. Miccio, A.M. Palmieri, R. Pecchioli, A. Romualdi and B.B. Shefton, Proceedings of 4th Symposium of the Hellenic Society for Archaeometry, Athens, 2003.

40 M. Ferretti, G. Cristoforetti, S. Legnaioli, V. Palleschi, A. Salvetti, E. Tognoni, E. Console and P. Palaia, *Spectrochim Acta B*, 2007, **62**, 1512-1518.

41 M. Ferretti, A. Gorghinian, S. Legnaioli, G. Lorenzetti and V. Palleschi, *Bollettino di Archeologia On Line II*, 2013, 2011/4, 65-72.

42 P. Binaghi, O. Colacicchi Alessandri, A. De Santis and M. Ferretti, Proceedings of Art'05, 8th International Conference on Non-Destructive Investigations and Microanalysis for the Diagnostics and Conservation of the Cultural and Environmental Heritage, Lecce, 2005.

43 M. Ferretti, G. Guida, N. Lucentini and F. Milazzo, Proceedings of 2nd International Conference on Archaeometallurgy in Europe, Aquileia, 2007.

44 M. Ferretti and S. Siano, *Appl Phys A-Mater*, 2008, **90**, 97-100.

45 S. Siano, J. Agresti, M. Ferretti, S. Mugnaini and M. Miccio, in *Donatello – Il David restaurato*, ed. B.P. Strozzi, Giunti, Firenze, 2008, pp. 168-183.

46 O. Colacicchi Alessandri, M. Ferretti and E. Formigli, in *Colore e luce nella statuaria antica in bronzo*, ed. E. Formigli, L'Erma di Bretschneider, Roma, 2013, pp. 25-31.

47 R. Cesareo, A. Brunetti and S. Ridolfi, *X-Ray Spectrom*, 2008, **37**, 309-316.

48 M. Ferretti, C. Polese and C. Roldán García, *Spectrochim Acta B*, 2013, **83-84**, 21-27.

49 M. Ferretti, G. Guida, N. Laschera and A. Manda, in Proceedings of the Conference Il tesoro di Misurata (Libia). Produzione e circolazione monetaria nell'età di Costantino il Grande, in press.

50 L.H. Cope, in *Methods of Chemical and Metallurgical Investigation of Ancient Coinage*, ed. E. T. Hall and D. M. Metcalf, RNS Special Publication 8. London, 1972, pp. 261-278.

51 D. Creagh, in *Physical techniques in the study of art, archaeology and cultural heritage*, ed. D. Creagh and D. Bradley, Elsevier, Amsterdam, 2007, vol.2, p. 42.

52 K. Janssens, in *Handbook of Spectroscopy*, ed. G. Gauglitz and T. Vo-Dinh, Whiley-VHC, Weinheim, 2003, vol. 1, p. 389.

53 K. Janssens, in *Non-destructive Micro Analysis of Cultural Heritage Materials*, ed. K. Janssens and R. Van Grieken, Elsevier, Amsterdam, 2004, p. 163.

54 G. Gilmore, *Practical Gamma-ray Spectroscopy*, John Wiley & Sons, 2nd edn., 2008, prgr. 4.4.4.

55 XR-100CR Si-PIN specification, http://www.amptek.com/pdf/xr100cr.pdf, (accessed March 2014).

56 A. Longoni and C. Fiorini, in *Handbook of Practical X-Ray Fluorescence Analysis*, ed. B. Beckhoff, B. Kanngießer, N. Langhoff, R. Wedell and H. Wolff, Springer-Verlag, Berlin, 2006, p. 221.

57 M. Ferretti, *Nucl Instrum Meth B*, 2004, **226**, 453-460.

58 R. Cesareo, M. Ferretti, G.E. Gigante, G. Guida, P. Moioli, S. Ridolfi and C. Roldán Garcia, *X-Ray Spectrom*, 2007, **36**, 167-172.

59 M. Mantler, in *Handbook of Practical X-Ray Fluorescence Analysis*, ed. B. Beckhoff, B. Kanngießer, N. Langhoff, R. Wedell and H. Wolff, Springer-Verlag, Berlin, 2006, 309-410.

60 T. Schoonjans, V.A. Solé, L. Vincze, M. Sanchez del Rio, K. Appel, C. Ferrero, *Spectrochim Acta B*, 2013, **82**, 36-41.

CAPTIONS TO FIGURES

Fig. 1

XRF investigation of a large bronze sculpture.

Fig. 2

Fraction of the overall fluorescent signal provided by a layer of depth *d* below the surface. The sample is a bronze alloy (85% Cu, 10% Sn, 5% Pb). The fluorescent lines considered are Cu-K, Sn-K and Pb-L. Almost the entire analytical information of Cu and Pb and almost half of the Sn information comes from the first 20μm.

Fig. 3

XRF spectrum of a bronze alloy containing 2.3% Sn, 3.4% Pb, 0.03% Ag and 0.15% Sb. Both the L- and the K-shells of Ag, Sn and Sb are excited, but the K-lines are more free from mutual interference than the L-lines.

Fig. 4

Pb mass fractions, on a logarithmic scale, of cast (black markers) and mechanically worked parts (white markers) in about 280 bronze artefacts from different cultural contexts (pre-Roman, Etruscan, Greek and Roman) and different ages (from 7th century B.C. to 1st century A.D.). Each object is identified by a progressive number on the horizontal axis. The objects are ordered by increasing Pb content to improve readability. Most white markers are below the corresponding black marker, meaning that, in the same object and independently on the absolute values, hammered parts always contain less Pb than the cast ones.

Fig. 5

SEM-BSE image of a cross-section. The grey level is related to the local mean atomic number. Pb has the highest atomic number and is represented with the lightest grey. The image shows the effect of annealing on a leaded bronze. At 600-700°C, Pb is liquid and tends to migrate towards the surface, where it is absorbed in the spongy layer of cupric oxide (CuO, tenorite).

Fig. 6

Model of the count-rates variations expected in a bronze substrate (88% Cu, 10% Sn, 2% Pb) covered by corrosion layers of irregular thickness, whose composition is given in Tab.1. The relative intensity is calculated as $RI(t)=I_{i,j}(t)/I_{i,0}$, where t is the coating thickness, $I_{i,j}(t)$ is the fluorescent intensity from the substrate and the corrosion layer, and $I_{i,0}$ is the fluorescent intensity from the substrate alone, the index i accounting for Cu-Kα, Sn-Kα or Pb-Lα, and the index j accounting for type I or type II corrosion. The model shows: a) an inverse relationship between the fluorescent intensity of Cu and those of Sn and Pb and b) surface concentrations of Sn (and Pb) several times higher than in the bulk.

Fig. 7

Scatterplot of the Sn versus Sb K-lines intensities measured on an artefact made of five separate pieces. The different alloys are identified as A, B, C, D and E. Three different compositional groups are distinguished: 1) alloys A, B and C, 2) alloy D and 3) alloy E.

Fig. 8

Histograms of the correlation coefficients between the count-rates of the main fluorescent lines. From top to bottom and from left to right the correlations are: Cu-Sn, Cu-Pb, As-Sn, Ag-Sn, Ag-Sb, Sn-Sb and Sn-Pb. The results refer to about 2500 XRF measurements carried out on the corroded surface of about 100 different alloys. The correlations among Ag, Sn and Sb are positive and high in most cases, whereas the correlations Cu-Sn and Cu-Pb are frequently negative.

Fig. 9

XRF analysis of the Capitoline Horse: scatterplot of the count-rates Sn vs. Sb. Only the left hind leg is in the cluster of the original alloy, whereas the other three legs, the brow and the tail form separated clusters. The outliers are marked with a grey circle.

Fig. 10

From top to bottom: SEM-BSE image, Ag map and Pb map of a specimen simulating a *nummus* alloy (Cu 88%, Sn 5%, Ag 3%, Pb 4%) after heating, before pickling. During heating a liquid phase of Pb and Ag migrates towards the surface, where Pb is oxidezed and takes the outer position, while Ag keeps closer to the bulk metal.

Fig. 11

Scatterplots of the areas of Pb Lα (top) and Ag L (bottom) lines versus Pb mass-fraction in the alloy the for specimens simulating *nummi* of different composition at each stage of the treatment. Surface Pb increases after heating and decreases after pickling. Ag is hidden by the overlaying Pb until the latter is removed. After the treatment, the surface amount of Ag is an increasing function of the Pb content in the alloy.

Fig. 12

Main components of an energy-dispersive XRF system.

Fig. 13

XRF spectrum of Cu at high count-rates: besides the Mo K-lines from the collimator, sum peaks can be observed at the energies: E(CuKα)+E(CuKα)=16.1keV, E(CuKα)+E(CuKβ)=16.95keV and E(CuKβ)+E(CuKβ)=17.8keV.

Fig. 14

Comparison on a logarithmic scale of the detection limits for Zn (red) and Sn (blue) for portable XRF systems having different X-ray tubes and detectors. The characteristics of each system are reported on the horizontal axis with the format: TubeHighVoltage_TubeCurrent_DetectorType. The acronyms SiPIN, SDD and HPGe refer to a SiPIN, a Si-Drift and a high-purity planar germanium detector, respectively.

Fig. 15

Absolute measurements versus compositional comparison in portable XRF investigation of ancient metal artefacts: the analytical approaches, the key aspects, the required features and the technical solutions that each option involves.

TABLES

Corrosion type	cuprite (Cu_2O) [%]	malachite ($Cu_2(CO_3)(OH)_2$) [%]	cassiterite (SnO_2) [%]	cerussite ($PbCO_3$) [%]
I	11	18	59	12
II	-	-	83	17

Tab. 1 Composition of the corrosion layers considered in the model, to simulate type I and type II corrosion patterns.

	Cu %	Sn %	Pb %	Zn %	Fe %	Ni %	Ag %	Sb %	As %	Bi %	Co %
Horse (front right hoof) Capitol 1064	82.5	5.7	13.2	0.005	0.02	0.018	0.02	0.15	0.02	0.006	bdl
Horse (brazing) Capitol 1064	73.5	7.5	17.8	0.005	0.01	0.02	0.018	0.05	0.025	0.003	0.07
Horse (right shoulder) Capitol 1064	87	9.3	3.1	bdl	0.09	0.04	0.02	0.02	0.06	0.004	0.015
Horse (head) Capitol 1064	86	8.8	3.5	bdl	0.37	0.05	0.02	0.02	0.06	0.015	0.02
Horse (left side) Capitol 1064	88	8.7	2.7	bdl	0.95	0.05	0.025	0.02	0.17	0.002	bdl
Horse (brazing) Capitol 1064	82	9.2	7.7	0.23	0.6	0.03	0.06	0.07	0.4	0.004	0.01
Horse (brazing) Capitol 1064	85	9.8	4.5	bdl	0.03	0.04	0.035	0.02	0.1	0.004	bdl

Tab. 2 Composition of the alloys of the Capitoline Horse as given in ref. 21, tab. 33 of the attached microfiches (*bdl* stands for 'below detection limits')

Detector type	Thickness [mm]	FWHM at 5.9keV [eV]	Shaping time [μs]	Count-rate capability [s^{-1}]
Nitrogen-cooled Si(Li)	5	165	4-10	10^4
Si-PIN	0.5	155-185	12-20	10^4
Si-Drift	0.45	150	1-2	10^5-10^6

Tab. 3 Typical figures of merit for nitrogen-cooled Si(Li), Si-PIN and Si-Drift detectors.

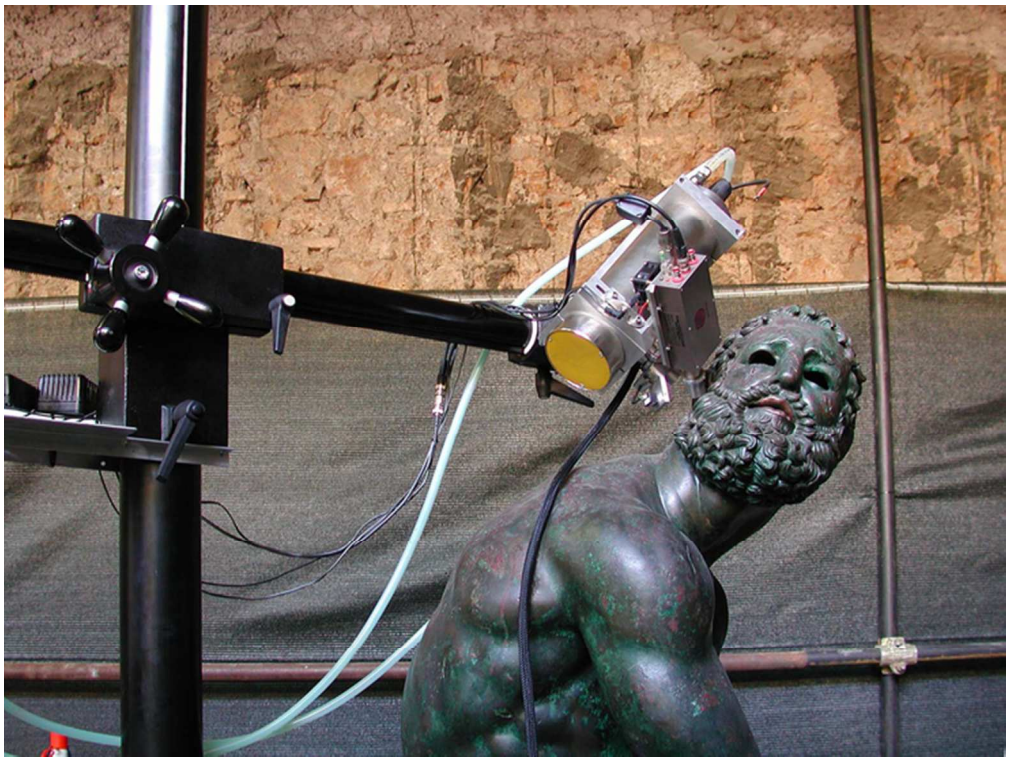

XRF investigation of a large bronze sculpture.
62x46mm (300 x 300 DPI)

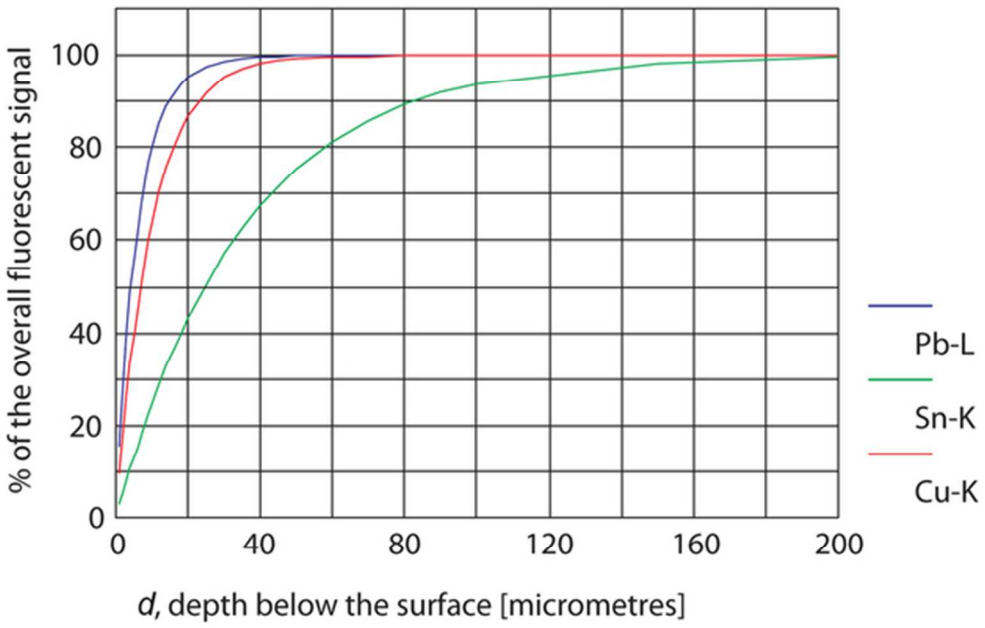

Fraction of the overall fluorescent signal provided by a layer of depth *d* below the surface. The sample is a bronze alloy (85% Cu, 10% Sn, 5% Pb). The fluorescent lines considered are Cu-K, Sn-K and Pb-L. Almost the entire analytical information of Cu and Pb and almost half of the Sn information comes from the first 20µm.
54x35mm (300 x 300 DPI)

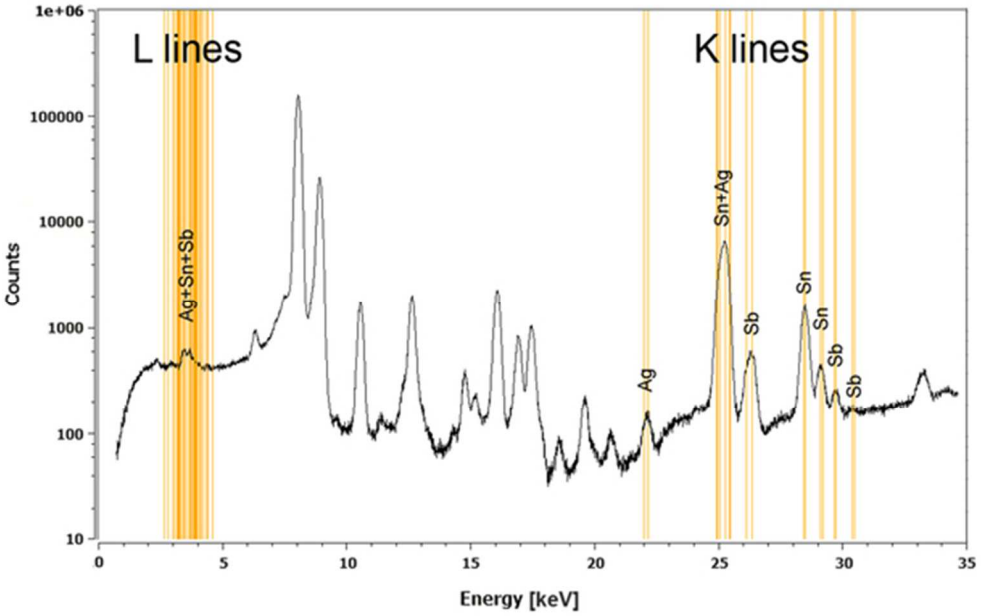

XRF spectrum of a bronze alloy containing 2.3% Sn, 3.4% Pb, 0.03% Ag and 0.15% Sb. Both the L- and the K-shells of Ag, Sn and Sb are excited, but the K-lines are more free from mutual interference than the L-lines.
52x33mm (300 x 300 DPI)

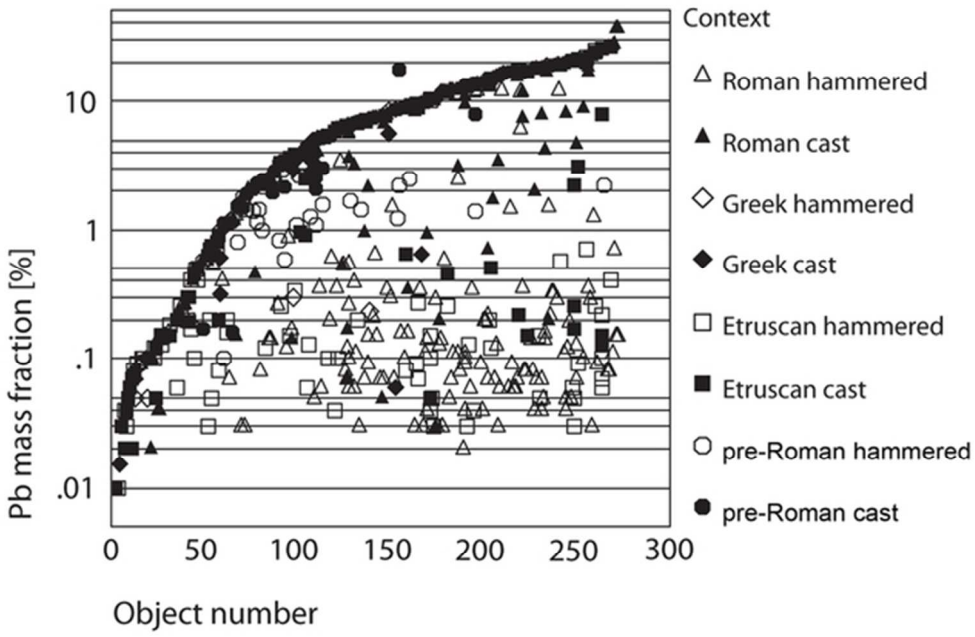

Pb mass fractions, on a logarithmic scale, of cast (black markers) and mechanically worked parts (white markers) in about 280 bronze artefacts from different cultural contexts (pre-Roman, Etruscan, Greek and Roman) and different ages (from 7th century B.C. to 1st century A.D.). Each object is identified by a progressive number on the horizontal axis. The objects are ordered by increasing Pb content to improve readability. Most white markers are below the corresponding black marker, meaning that, in the same object and independently on the absolute values, hammered parts always contain less Pb than the cast ones.
55x36mm (300 x 300 DPI)

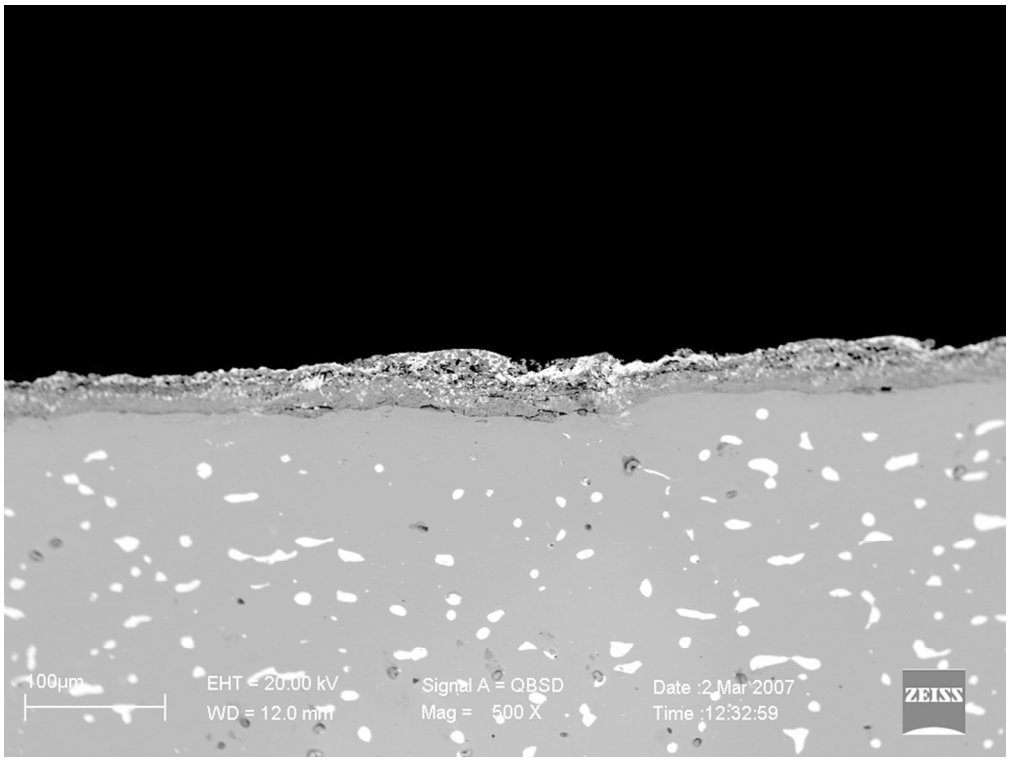

SEM-BSE image of a cross-section. The grey level is related to the local mean atomic number. Pb has the highest atomic number and is represented with the lightest grey. The image shows the effect of annealing on a leaded bronze. At 600-700°C, Pb is liquid and tends to migrate towards the surface, where it is absorbed in the spongy layer of cupric oxide (CuO, tenorite).
90x67mm (300 x 300 DPI)

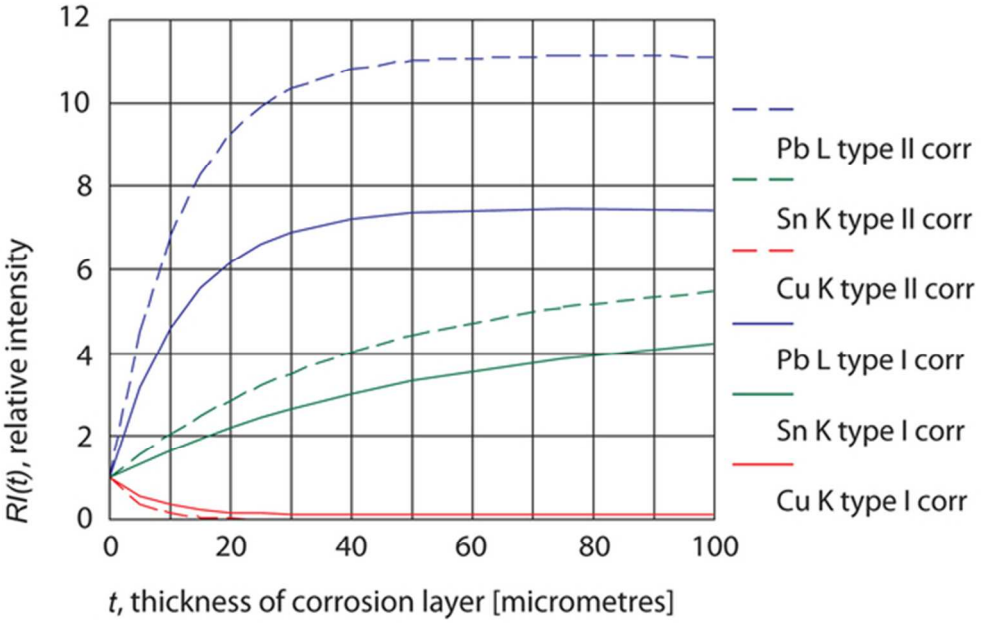

Model of the count-rates variations expected in a bronze substrate (88% Cu, 10% Sn, 2% Pb) covered by corrosion layers of irregular thickness, whose composition is given in Tab.1. The relative intensity is calculated as $RI(t)=I_{i,j}(t)/I_{i,0}$, where t is the coating thickness, $I_{i,j}(t)$ is the fluorescent intensity from the substrate and the corrosion layer, and $I_{i,0}$ is the fluorescent intensity from the substrate alone, the index i accounting for Cu-Kα, Sn-Kα or Pb-Lα, and the index j accounting for type I or type II corrosion. The model shows: a) an inverse relationship between the fluorescent intensity of Cu and those of Sn and Pb and b) surface concentrations of Sn (and Pb) several times higher than in the bulk.
54x35mm (300 x 300 DPI)

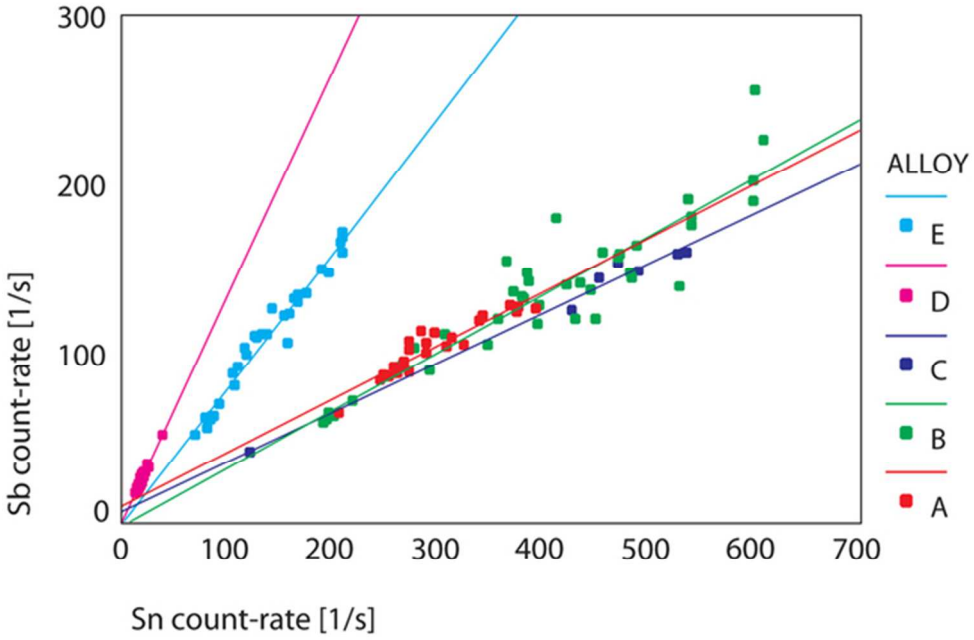

Scatterplot of the Sn versus Sb K-lines intensities measured on an artefact made of five separate pieces. The different alloys are identified as A, B, C, D and E. Three different compositional groups are distinguished: 1) alloys A, B and C, 2) alloy D and 3) alloy E.
56x38mm (300 x 300 DPI)

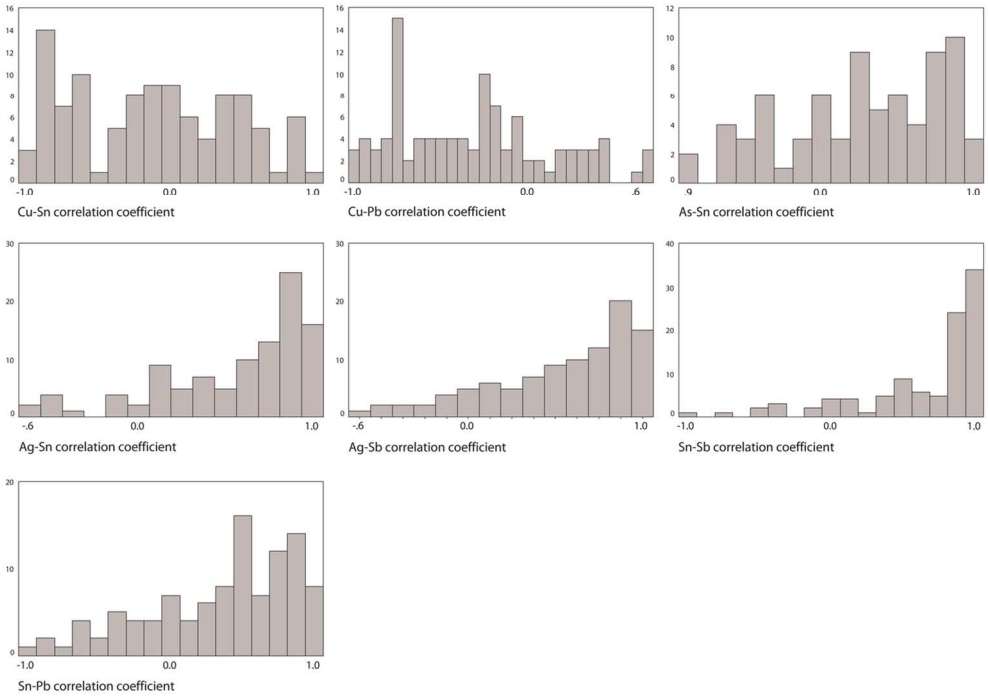

Histograms of the correlation coefficients between the count-rates of the main fluorescent lines. From top to bottom and from left to right the correlations are: Cu-Sn, Cu-Pb, As-Sn, Ag-Sn, Ag-Sb, Sn-Sb and Sn-Pb. The results refer to about 2500 XRF measurements carried out on the corroded surface of about 100 different alloys. The correlations among Ag, Sn and Sb are positive and high in most cases, whereas the correlations Cu-Sn and Cu-Pb are frequently negative.
121x85mm (300 x 300 DPI)

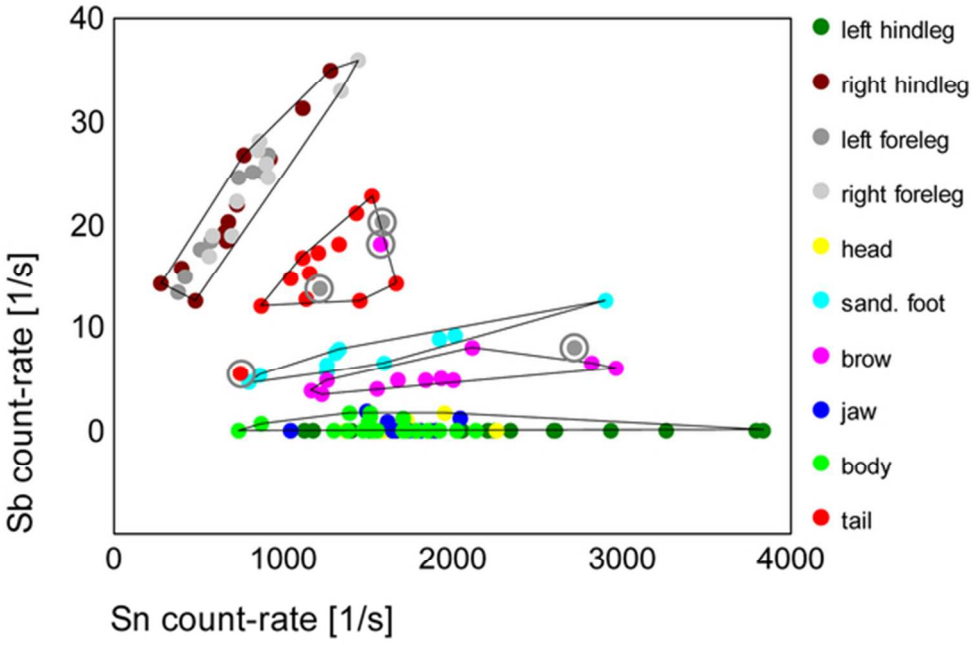

XRF analysis of the Capitoline Horse: scatterplot of the count-rates Sn vs. Sb. Only the left hind leg is in the cluster of the original alloy, whereas the other three legs, the brow and the tail form separated clusters. The outliers are marked with a grey circle.
55x37mm (300 x 300 DPI)

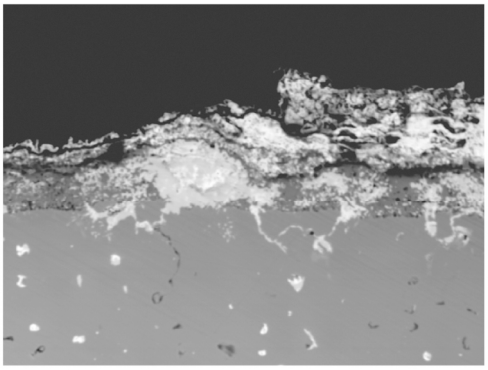

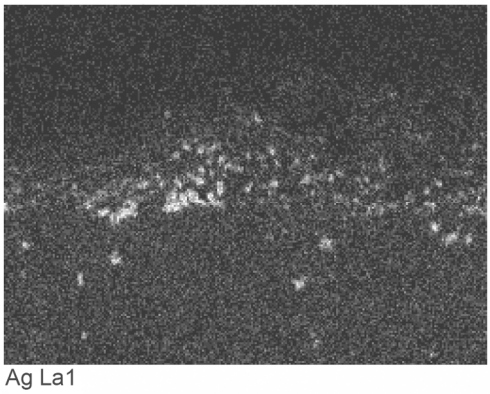

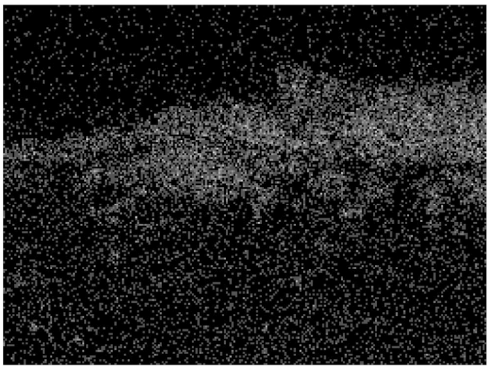

From top to bottom: SEM-BSE image, Ag map and Pb map of a specimen simulating a *nummus* alloy (Cu 88%, Sn 5%, Ag 3%, Pb 4%) after heating, before pickling. During heating a liquid phase of Pb and Ag migrates towards the surface, where Pb is oxidezed and takes the outer position, while Ag keeps closer to the bulk metal.
84x205mm (300 x 300 DPI)

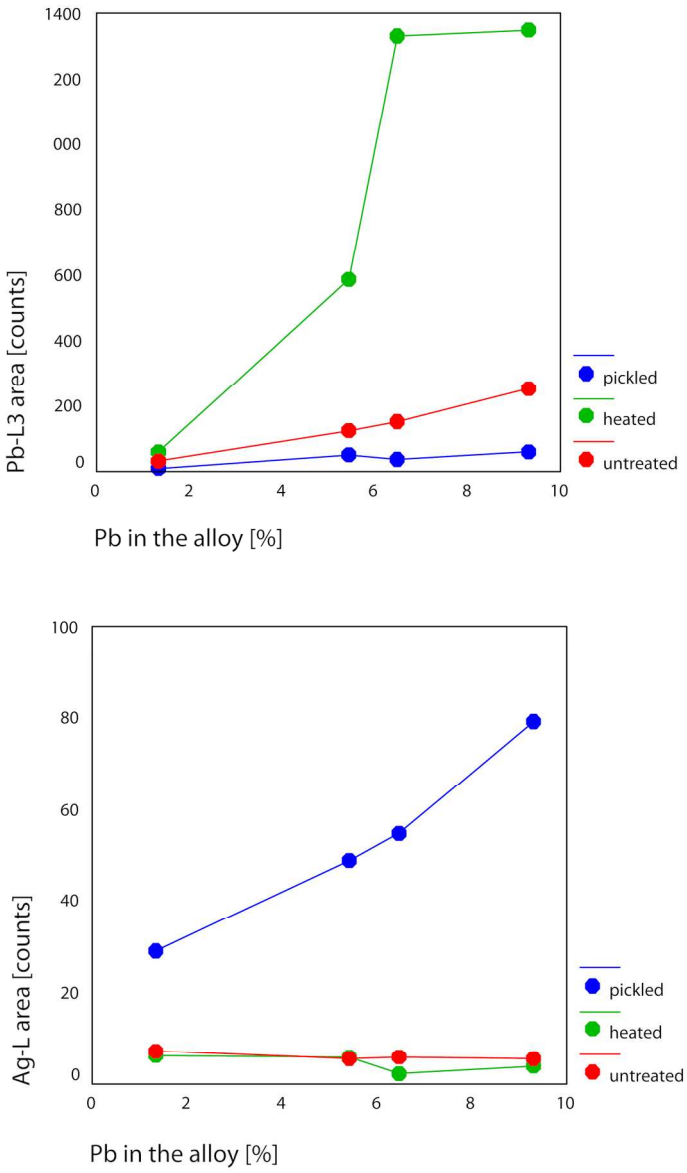

Scatterplots of the areas of Pb Lα (top) and Ag L (bottom) lines versus Pb mass-fraction in the alloy the for specimens simulating *nummi* of different composition at each stage of the treatment. Surface Pb increases after heating and decreases after pickling. Ag is hidden by the overlaying Pb until the latter is removed. After the treatment, the surface amount of Ag is an increasing function of the Pb content in the alloy.
137x227mm (300 x 300 DPI)

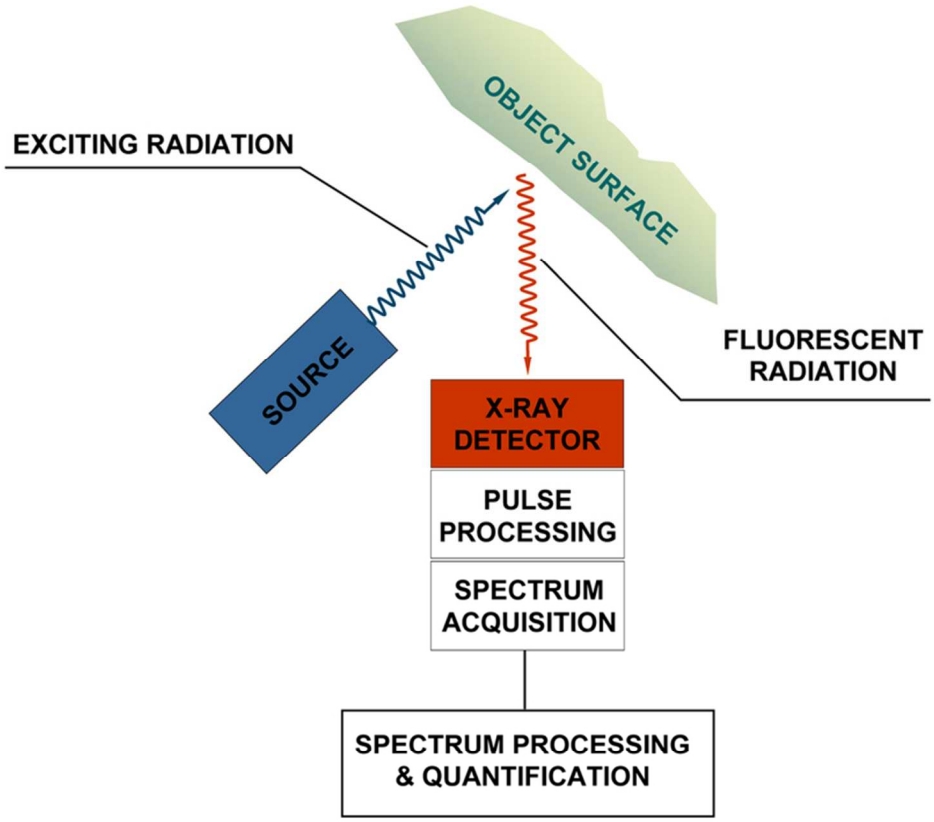

Main components of an energy-dispersive XRF system.
73x64mm (300 x 300 DPI)

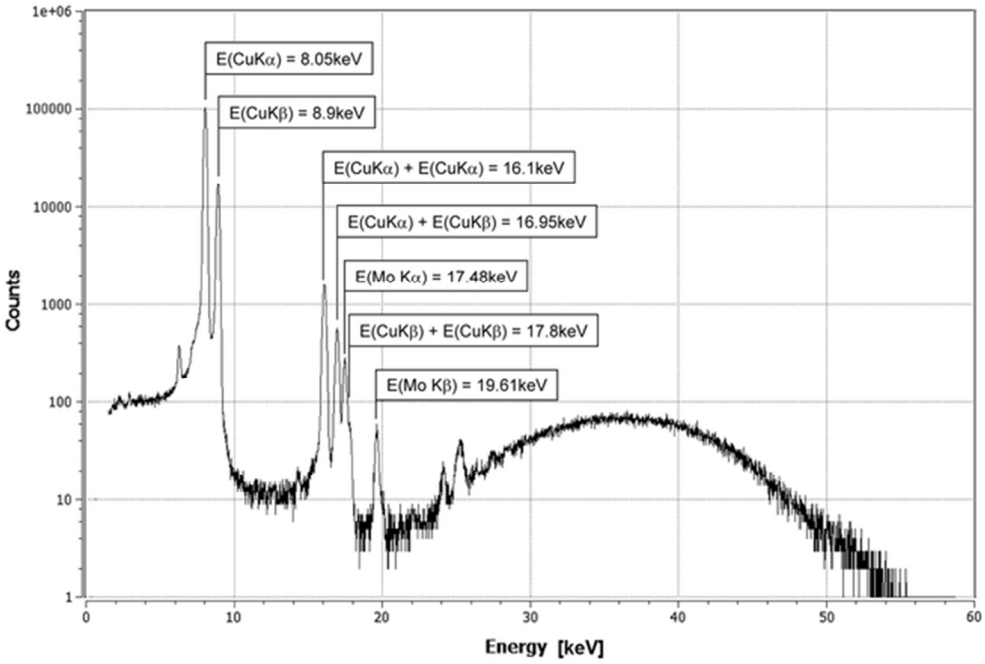

XRF spectrum of Cu at high count-rates: besides the Mo K-lines from the collimator, sum peaks can be observed at the energies: E(CuKα)+E(CuKα)=16.1keV, E(CuKα)+E(CuKβ)=16.95keV and E(CuKβ)+E(CuKβ)=17.8keV.
56x38mm (300 x 300 DPI)

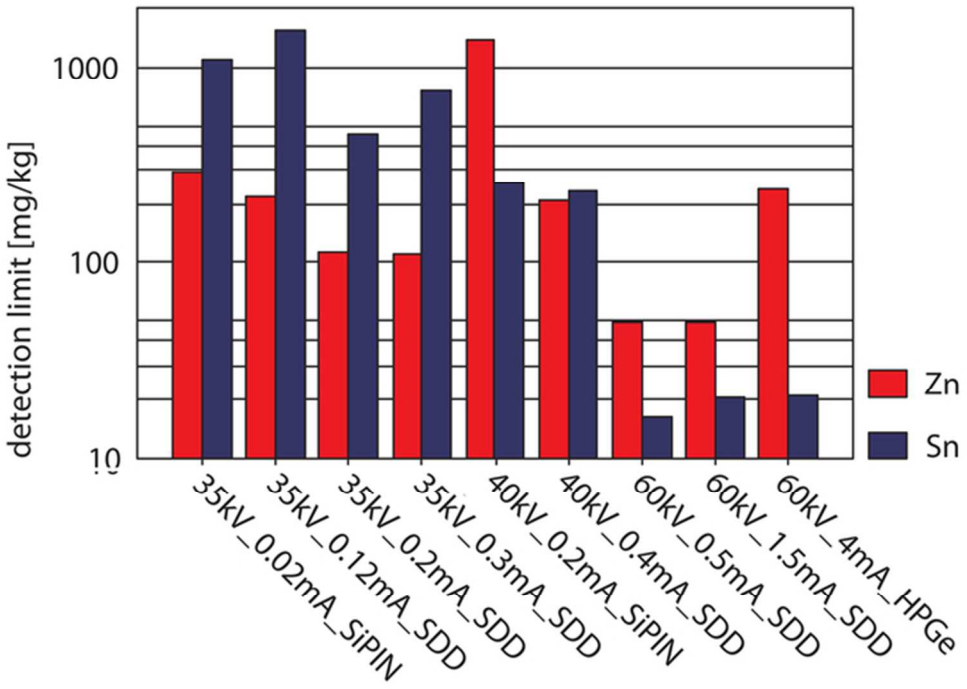

Comparison on a logarithmic scale of the detection limits for Zn (red) and Sn (blue) for portable XRF systems having different X-ray tubes and detectors. The characteristics of each system are reported on the horizontal axis with the format: TubeHighVoltage_TubeCurrent_DetectorType. The acronyms SiPIN, SDD and HPGe refer to a SiPIN, a Si-Drift and a high-purity planar germanium detector, respectively.
60x43mm (300 x 300 DPI)

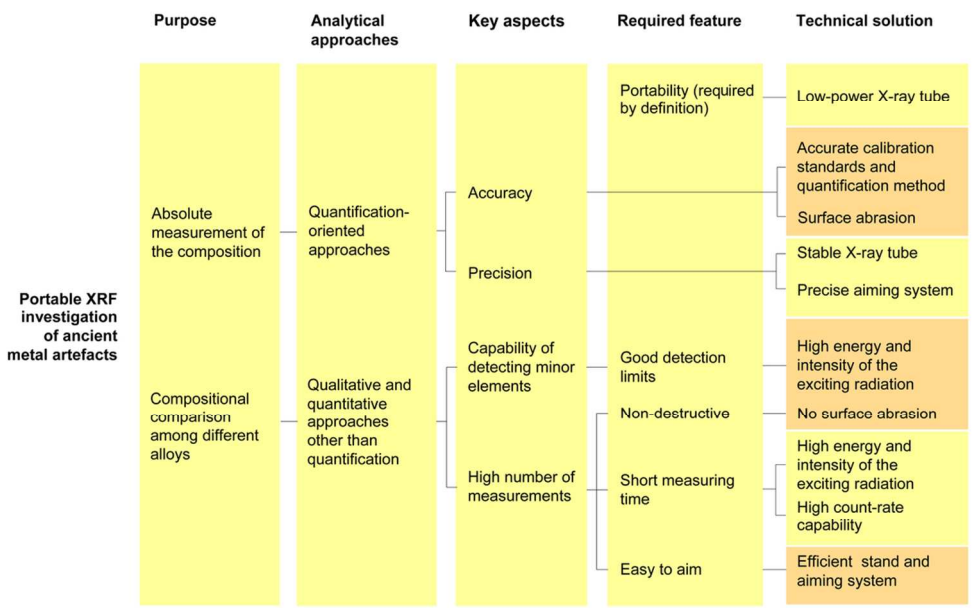

Absolute measurements versus compositional comparison in portable XRF investigation of ancient metal artefacts: the analytical approaches, the key aspects, the required features and the technical solutions that each option involves.
107x67mm (300 x 300 DPI)